E-SAR P-band System Performance

Ralf Horn, Rolf Scheiber, Bernd Gabler, Markus Limbach
Microwaves & Radar Institute, German Aerospace Center (DLR), Germany

Abstract

DLR's experimental airborne SAR E-SAR is well-known in Europe and beyond. It is a versatile system operating in four major radar frequency bands, one of them being the P-band starting at 300MHz. While the DLR is successfully operating the P-band E-SAR under operational conditions for a couple of years now after having finished the development of a new antenna, not much has been published so far about the performance of the system. In this paper the design of the P-band radar sub-system is reviewed and results of a performance analysis are presented.

1 Introduction

Synthetic Aperture Radar in comparison to standard radar systems offers the possibility to obtain high resolution even at low frequencies (f_c<1GHz). Special signal processing algorithms are available to process range bandwidths of 20 to 30% of the centre frequency and more. Existent antenna technology allows the design of antennas which feature large bandwidths and good radiometric and polarimetric performance the same time. The frequency band designations (P, L, S, C, X) of World War II are still the most commonly used. According to that "P" stands for the frequency range 300 - 1000MHz (or 30 - 100cm wavelength) [1].
The low end of the P-band (300 - 400MHz) in particular is very attractive for several reasons:

a) *Minimum RF interference from external radio transmitters.* The frequency range above 400MHz is clustered with numerous broadcasting transmitters creating serious problems in normal SAR operation. RF interference degrades image quality dramatically as we have experienced and in the majority of the cases filtering the RFI did not succeed.

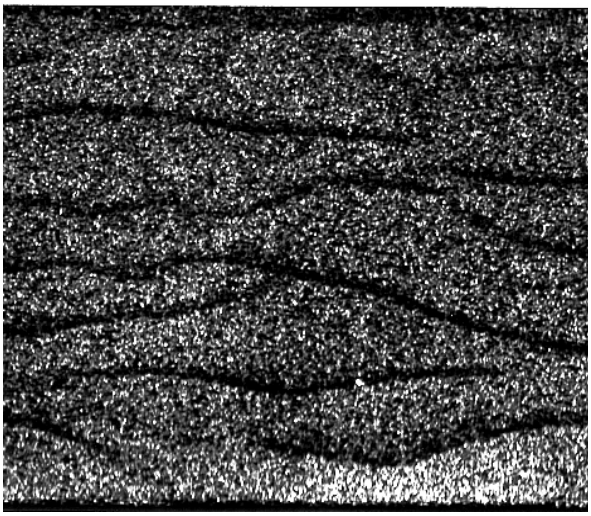

Figure 1 Sea bottom topography near Hoek van Holland (NL), obtained with E-SAR P-band in HH polarisation in the frame of the 1996 C-STAR experiment.

b) *Simple radar design.* RF components are available for building a simple wideband SAR RF front-end. Standard AD-conversion with 6 or 8bits per sample can be employed.

Application specific benefits:

a) *Oceanography.* P-band radar is very susceptible to bathymetric and oceanographic features displayed on sea surface, like for example sea bottom topography as shown in **Figure 1**.

b) *Glaciology.* Signal attenuation in ice at 350MHz is low compared to higher frequencies like L-band. According to Evans & Smith [2] the dielectric loss coefficient of ice at a temperature of -30°C at P-band is ca. 1dB/100m. At L-band (1.3GHz) it is ca. 10dB/100m. This makes P-band suitable for measurements on polar ice sheets and glaciers.

c) *Forestry and military applications.* P-band compared to L-band has improved foliage penetration and hence target detection under forest canopy capabilities. Applying Pol-InSAR or SAR tomography techniques one can obtain improved results in forest height and in volumetric imaging.

However, operation of a P-band SAR in the range of 300 - 400MHz, has also critical points. The frequency range is occupied mainly by military communications and the glideslope of the Instrument Landing System (ILS) at airports (328.6 - 335.4MHz). A study is being conducted to investigate if and to which degree the E-SAR P-band is interfering with these services.

2 E-SAR P-band RF section design reviewed

The E-SAR P-band section consists of the main building blocks "converter and front-end" and "antenna". Both are reviewed here. For more details refer to [3].

2.1 P-band converter and front-end

In E-SAR the radar signal is a down-chirped pulse with 100MHz maximum bandwidth and 5µs pulse length. The centre frequency is 300MHz. The signal chirps from 350MHz to 250MHz, which is overlapping with the desired P-band frequency range. Neither direct transmission nor direct conversion are possible. The workaround is to first up-convert the radar chirp into L-band (f_c = 1.3GHz) and then down-convert to 350MHz centre frequency. For down-conversion a programmable phase-locked-oscillator is used, so that the P-band centre frequency is adjustable from 350MHz to 370MHz.

The P-band front-end has a classical design (**Figure 3**). A solid state amplifier generates 1kW of transmit peak power. A passive circulator separates transmit and receive paths. A PIN switch is used to switch antenna polarisation pulse-to-pulse. The isolation of the switch is better than 60dB. The front-end is designed to handle 10% duty cycle at a maximum PRF of 12kHz.

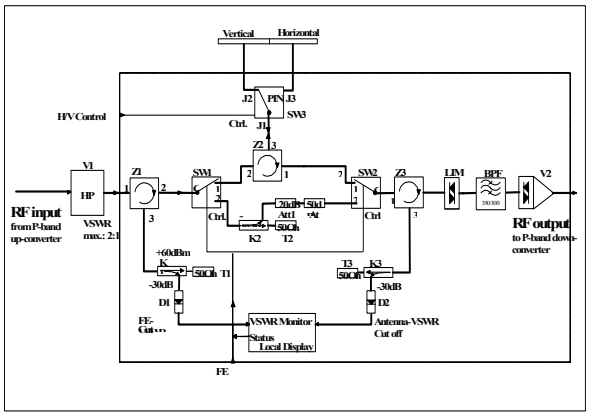

Figure 3 P-band front-end blockdiagram.

2.2 Antenna characteristics

The antenna is a 16-element microstrip patch array set up in four groups. The single element consists of triple stacked resonators. The feed network introduces a combined amplitude and phase taper to achieve the desired radiation characteristics. Azimuth beamwidth is ca. 30° in both H and V polarisation. Sidelobes are 15dB down. Elevation beamwidth is 39° and 40° for H and V polarisation, respectively (**Figure 4**). Antenna gain at f_c is 12dBi in V and 8dBi in H. The achieved bandwidth is 100MHz or 28% of f_c. Cross-polarisation isolation is equal or better than 20dB.

The P-band antenna is mounted flat under the fuselage in front of the main gear of the aircraft (**Figure 5**) as the only possible location. Suitable hardpoints support the antenna's weight of 136kg including the windshield. Looking at the elevation beam pattern, we notice an unwanted opposite swath illumination of ca. 25dB below the 2-way main beam maximum. This fact must be well considered in P-band SAR measurements.

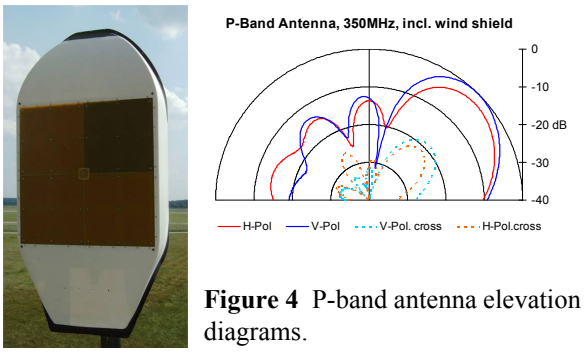

Figure 4 P-band antenna elevation diagrams.

Figure 5 E-SAR onboard DLR's Dornier DO228-212 aircraft touching down after a successful measurement flight.

2.3 Laboratory measurements

Each time we install E-SAR in the aircraft calibration measurements are performed in the laboratory. Parameters like transmit power, receiver gain and noise figure are measured. In **Figure 6** an example for P-band is shown. The gain of the receiver section totals to 84 dB and the noise figure (excl. antenna) results to 4.5dB.

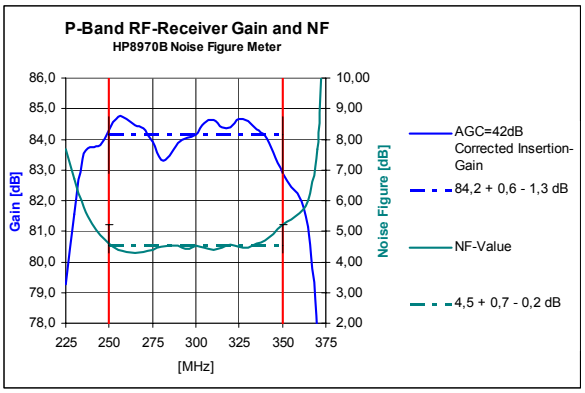

Figure 6 Example of P-band receiver gain and noise figure measurement.

3 Imaging performance analysis

First radiometric and polarimetric data calibration was implemented already after first flight tests in 2003. A

more refined radiometric calibration could be implemented using data of the 2004 INDREX campaign [4] to account better for small antenna pattern distortions. In addition to that some data sets were extremely useful for a general imaging performance analysis of P-band. The results are presented here.

3.1 Refined radiometric calibration

One of the test sites (MAWAS) covered during the INDREX campaign is characterized by extremely homogeneous peat swamp forest. This site was used to refine the radiometric accuracy of all E-SAR antenna patterns deployed during this campaign. Especially for P-band it is extremely difficult to obtain reliable calibration, as corner reflectors of suitable size are very difficult to deploy and homogeneous areas of known reflectivity are hard to find at temperate latitudes. **Figure 7** shows the initial estimate of $\gamma = \sigma^0 / \cos\theta_i$ as a function of incidence angle, estimated from a flat area of homogeneous tropical rain forest. The spike in HH polarisation stems from a long wooden pathway in the test site, running exactly parallel to the flight direction (image on the right of **Figure 7**).

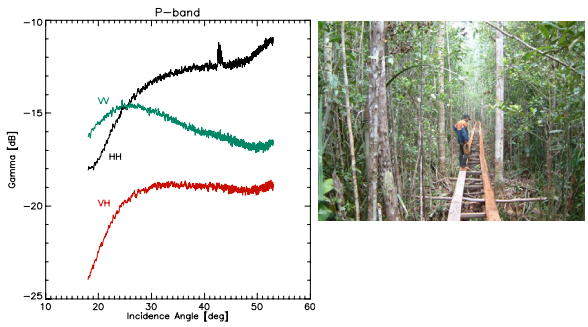

Figure 7 Initial estimates of P-band radar reflectivity γ. A wooden pathway (parallel to the flight direction, at 43° off-nadir) scatters strongly in HH.

Assuming constant γ as a function of incidence angle, this variation was filtered and used for proof of radiometry on corner reflectors. The match was perfect for HH polarisation, however for the VV polarisation a variation of 1.1dB remained comparing the RCS of near and far range corner reflectors.
It was decided to trust the CR signatures and an additional linear compensation was included from near to far range for VV. We attribute this difference to an increase of surface scattering contribution at steep incidence angles, which contradicts the assumption of constant γ. Note also, that nominal incidence angles for the P-band antenna start at 25° off-nadir.

3.2 Nadir echoes

Due to antenna design constraints there is no explicit Null of the antenna pattern in nadir direction. This leads to strong nadir reflections, especially in HH polarisation. Specular reflection occurs over smooth surfaces, especially in case of open water. In some cases the resulting side-lobes of the range compressed signal deteriorate near-range parts of the image (see **Figure 9**), especially if incidence angles less than 25° are of interest (like for INDREX data). Nadir ambiguities may also occur in other parts of the image, especially when sampling in range at the Nyquist limit.

3.3 Estimation of NESZ

Two methods were adopted for the quantification of the noise level in P-band image data. The first method evaluates an area of smooth open water at approx. 40° off-nadir, as indicated in **Figure 9**. The level estimated this way equals to -34dB in HH and VV polarisation and -32dB for HV. An alternative method estimates the noise level in the pre-nadir region of the image, N_{pre_nadir}, and extrapolates the value to different incidence angles as a function of calibration factors applied during the processing (this way accounting for antenna diagram and two-way propagation attenuation).

$$NESZ(\theta_i) = N_{pre\_nadir} \cdot CAL(\theta_i) / CAL_{pre\_nadir} \cdot \sin\theta_i$$

For P-band this estimation may be biased, particularly in HH, due to the high energy level in nadir echo sidelobes. **Figure 8** shows the NESZ obtained this way from a data set without water in nadir direction. Only in HH and VV the values roughly confirm those obtained across the dark image areas, whereas HV is better by 6dB compared to VV (better by 8 dB compared to previous method). We conclude, that NESZ across the nominal incidence angle range is definitely better than -30dB.

3.4 Opposite swath suppression

For the same reason as for the nadir echoes opposite swath radar returns cannot be fully suppressed. The performance of the antenna was evaluated using the same data set of **Figure 9**, where opposite swath content is clearly visible in open water areas. The opposite swath attenuation within the image is evaluated at two

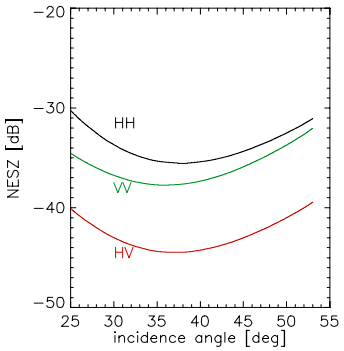

Figure 8 NESZ for the different P-band polarisations as a function of incidence angle

different off-nadir angle ranges, as summarised in Table 1. Areas in water are compared to areas on land at the same incidence angle range, assuming similar backscatter intensity. Compared to the measured antenna patterns this corresponds well for the higher incidence angles (in VV regular backscatter from open water biases the estimation), but performance is worse by 6-10dB for the near range. Further inspection of the area showed, that the near range opposite swath corresponds to the harbour and sub-urbs of Balikpapan city, with probably higher backscatter than the reference areas, which explains the observation. However, the antenna properties should be considered for campaign planning in the future, to avoid undesired effects.

Table 1 Estimated opposite swath ambiguity levels

Off-nadir\ Polarisation	HH	VV	HV
27-37° (from image)	-12dB	-12dB	-16dB
42-46° (from image)	-21dB	-17dB	-19dB
From antenna pattern	< -20dB		

3.5 RF interferences

So far strong effects caused by RF-interference were noticed only in very close vicinity to airports (ILS influence). All other data acquired (in Austria, Switzerland, Indonesia) were not or only marginally affected in cross-polarisation. In these few cases RFI-filtering was successful.

3.6 Interferometric performance

For interferometry the implication of limited opposite swath attenuation is mainly an additional source of noise (at least for baselines different from 0m). According to $\gamma_{opp}=SNR/(1+SNR)$, -12dB corresponds to a coherence contribution of $\gamma_{opp}=0.94$. However, inspection of several P-band interferometric pairs proved that average(!) coherence levels in case of small baselines are often above 0.96 (including SNR, opposite swath, temporal & volumetric decorrelation). We therefore conclude that opposite swath attenuation is well described by the antenna pattern, i.e. in the order of -20 to -25dB.

4 Conclusions

E-SAR's 300 - 400MHz P-band sub-system allows the acquisition of image data of very good quality. The radar resolution is typically 2.3m in slant range and 2m (single look) in azimuth direction. This has been demonstrated in several missions. The excellent performance, which could be achieved due to the fact that the frequency band chosen is restricted in use, is only limited by the antenna characteristics which cannot be improved much and the dynamic range of the AD-converters which determine the achievable image contrast. Hence, employing the P-band sensor requires careful site planning to keep opposite swath backscatter levels low and target backscatter dynamics in limits.

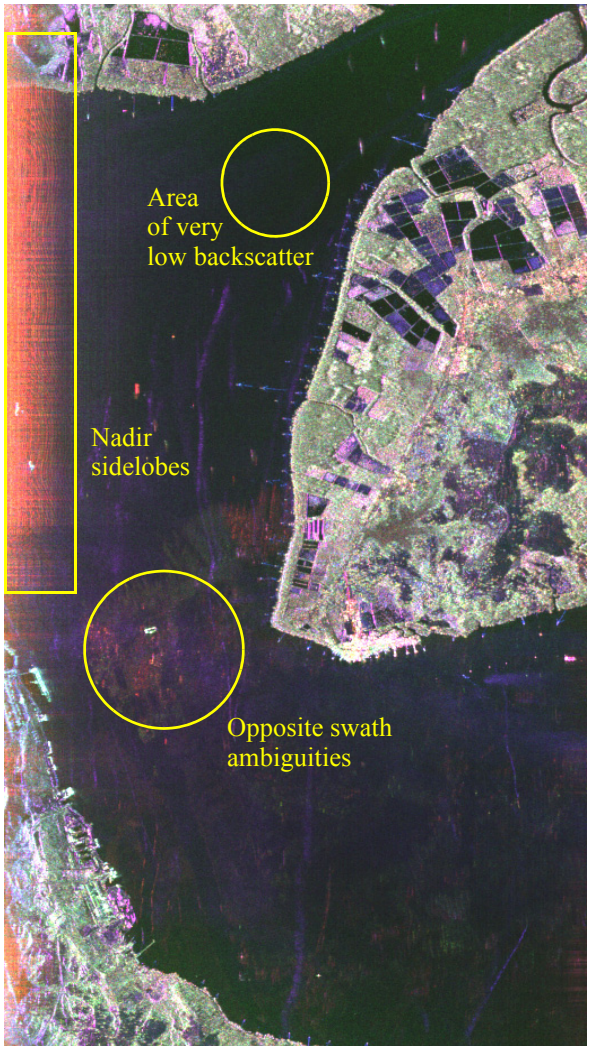

Figure 9 P-band polarimetric composite (RGB=HH-HV-VV) showing performance limitations: Nadir sidelobes at angles < 18° & opposite swath ambiguities.

References

[1] Long, Maurice W.: *Radar Reflectivity of Land and Sea*, 2nd edition, Artech House, Inc, 1983

[2] Evans, S., Smith, B. M. E.: *A radio echo equipment for depth sounding in polar ice sheets*, Journal of Scientific Instruments (Journal of Physics E), Series 2, Vol. 2, 1969

[3] Limbach, M., Gabler, B., Horn, R.: *Fine Resolution, fully Polarimetric P-band Sub-system for E-SAR - Technique and Results*, 5th EUSAR 2004, Ulm, Germany, VDE Verlag, 2004, S. 275 - 278

[4] Hajnsek, I., et al.: *INDREX II - Indonesian Airborne Radar Experiment Campaign over Tropical Forest in L- and P-band*, Proc. of 2nd Pol-InSAR Workshop, Frascati, January, 2005